

# Investigation on Fluid Flow Characteristics of the Orifice in Nuclear Power Plant

Nam-Seok Kim, Sang-Kyu Lee, Byung-Soo Shin, and O-Hyun Keum

**Abstract**—The present paper represents a methodology for investigating flow characteristics near orifice plate by using a commercial computational fluid dynamics code. The flow characteristics near orifice plate which is located in the auxiliary feedwater system were modeled via three different levels of grid and four different types of Reynolds Averaged Navier-Stokes (RANS) equations with proper near-wall treatment. The results from CFD code were compared with experimental data in terms of differential pressure through the orifice plate. In this preliminary study, the Realizable  $k$ - $\epsilon$  and the Reynolds stress models with enhanced wall treatment were suitable to analyze flow characteristics near orifice plate, and the results had a good agreement with experimental data.

**Keywords**—Auxiliary Feedwater, Computational Fluid Dynamics, Orifice, Nuclear Power Plant

## I. INTRODUCTION

THE calculation of fluid flow rate by measuring the pressure difference across a pipe restriction is perhaps the most commonly used flow measurement technique in industrial application including nuclear fields. Because of the availability for all pipe sizes and the cost effectiveness for measuring flow rate in larger pipes (over 6" diameter), the orifice flowmeter is widely used in the nuclear power plant. These kinds of orifice flowmeter shall be installed in the pipeline at a position such that the flow conditions immediately upstream sufficiently approach those of a fully developed profile and are free from swirl. As there are many guidelines for installation requirements of these kinds of flowmeter, such as ASME PTC 19.5 ([1],[2]), it's not always easy to conclude whether the flow conditions are sufficiently fully developed or not. Especially, whenever piping arrangements are complicated, it is necessary to analyze flow characteristics nearby the primary element like orifice plate.

In this point of view, Computational Fluid Dynamics (CFD) method is suitable for investigating the influence of the complex geometry. For applying CFD, the proper selections of grid level and turbulence model are important to describe fluid motions. However, no single turbulence model with fixed grid size is universally accepted as being superior for all classes of problems. The choice of turbulence model depends on

considerations such as the physics encompassed in the flow, the established practice for a specific class of problem, the level of accuracy required, the available computational resources, and the amount of time available for the simulation. [3] All these things depend on user's experience with a lot of time spent.

The present study aims at drawing up recommendations for choosing appropriate grid levels and turbulence models to well describe flow characteristics through the orifice plate in the auxiliary feedwater system of nuclear power plant. Three different levels of grid and four types of turbulence models were evaluated using commercial computational fluid dynamics code (Fluent v.6.2).

## II. ORIFICE IN AUXILIARY FEEDWATER SYSTEM

The auxiliary feedwater system in nuclear power plant is a safety related system that maintains an inventory in the secondary side of the steam generators to ensure a heat sink for the removal of reactor decay heat. Thus, the proper operation of the auxiliary feedwater system is critical for the prevention of core melt in the pressurized water reactors, and maintaining the performance of auxiliary feedwater pumps is important. [4]

For this reason, there is a recirculation line in the auxiliary feedwater system for testing and verifying a performance of the auxiliary feedwater pumps, and measuring a flow rate by using the orifice flowmeter. The simple geometry for the recirculation line in the auxiliary feedwater system is illustrated in Fig. 1.

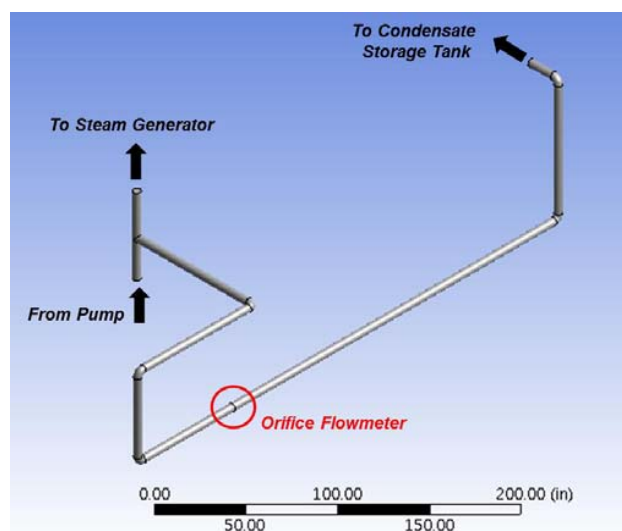


Fig. 1 Simple geometry for recirculation line in AFWS

Nam-Seok Kim is with Korea Institute of Nuclear Safety, Guseong, Yuseong, Daejeon, 305-338, Republic of Korea (e-mail: nskim@kins.re.kr)

Sang-Kyu Lee is with Korea Institute of Nuclear Safety, Guseong, Yuseong, Daejeon, 305-338, Republic of Korea (e-mail: sklee@kins.re.kr)

Byung-Soo Shin is with Korea Institute of Nuclear Safety, Guseong, Yuseong, Daejeon, 305-338, Republic of Korea (e-mail: k975sbs@kins.re.kr)

Oh-Hyun Keum is with Korea Institute of Nuclear Safety, Guseong, Yuseong, Daejeon, 305-338, Republic of Korea (e-mail: k092koh@kins.re.kr)

### III. TURBULENCE MODELS

Turbulence models considered in this study are based on RANS (Reynolds Averaged Navier-Stokes) equations. [5] In RANS model, the solution variables in the instantaneous Navier-Stokes equations are decomposed into the averaged and fluctuating components. Transport equations using the time averaged quantities result in the Reynolds-averaged equations below. The bar usually denoting the time-averaged quantities were dropped, except for products of fluctuating quantities.

$$\frac{\partial \rho}{\partial t} + \frac{\partial}{\partial x_i}(\rho u_i) = 0 \quad (1)$$

$$\frac{\partial}{\partial t}(\rho u_i) + \frac{\partial}{\partial x_j}(\rho u_i u_j) =$$

$$-\frac{\partial p}{\partial x_i} + \frac{\partial}{\partial x_j} \left[ \mu \left( \frac{\partial u_i}{\partial x_j} + \frac{\partial u_j}{\partial x_i} - \frac{2}{3} \delta_{ij} \frac{\partial u_k}{\partial x_k} \right) \right] + \frac{\partial}{\partial x_j}(-\rho \overline{u_i' u_j'})$$

The Reynolds stress term,  $\rho \overline{u_i' u_j'}$  in Eq.(2) that was from the non-linear convective term in the un-averaged equation, reflects the fact that convective transport due to turbulent velocity fluctuations will act to enhance mixing over and above that caused by fluctuations at the molecular level. It needs to be modeled to close the system of equations.

A common method employs the Boussinesq hypothesis to relate the Reynolds stresses to the mean velocity:

$$-\rho \overline{u_i' u_j'} = \mu_t \left( \frac{\partial u_i}{\partial x_j} + \frac{\partial u_j}{\partial x_i} \right) - \frac{2}{3} \left( \rho k + \mu_t \frac{\partial u_k}{\partial x_k} \right) \delta_{ij} \quad (3)$$

where  $\mu_t$  is the turbulent viscosity. This approach has the advantage of relatively low computational cost associated with the computation of  $\mu_t$ , though it assumes  $\mu_t$  is an isotropic scalar quantity, which is not strictly true.

The alternative approach, embodied in the Reynolds Stress Models, is to solve transport equations for each of the terms in the Reynolds stress tensor. In this study, three Boussinesq hypotheses and one Reynolds stress approaches are employed.

#### A. The Standard k-ε Model

The standard k-ε model is a semi-empirical model based on model transport equations for the turbulence kinetic energy (k) and its dissipation rate (ε) as below.

$$\frac{\partial}{\partial t}(\rho k) + \frac{\partial}{\partial x_i}(\rho k u_i) = \frac{\partial}{\partial x_j} \left[ \left( \mu + \frac{\mu_t}{\sigma_k} \right) \frac{\partial k}{\partial x_j} \right] + G_k + G_b - \rho \varepsilon - Y_M \quad (4)$$

$$\frac{\partial}{\partial t}(\rho \varepsilon) + \frac{\partial}{\partial x_i}(\rho \varepsilon u_i) = \frac{\partial}{\partial x_j} \left[ \left( \mu + \frac{\mu_t}{\sigma_\varepsilon} \right) \frac{\partial \varepsilon}{\partial x_j} \right] + C_{1\varepsilon} \frac{\varepsilon}{k} (G_k + C_{3\varepsilon} G_b) - C_{2\varepsilon} \rho \frac{\varepsilon^2}{k} \quad (5)$$

where  $C_{1\varepsilon}$ ,  $C_{2\varepsilon}$ ,  $\sigma_k$ , and  $\sigma_\varepsilon$  are empirical constants,  $G_k$  and  $G_b$  are a generation term for turbulence, and  $Y_M$  is the contribution of the fluctuating dilatation in compressible turbulence to the overall dissipation rate.

The turbulence viscosity of the k-ε model is linked to the

turbulence kinetic energy and dissipation via the relation

$$\mu_t = \rho C_\mu \frac{k^2}{\varepsilon} \quad (6)$$

where  $C_\mu$  is a value of 0.09, which is taken from experimental data.

#### B. The Realizable k-ε Model

The realizable k-ε model contains an alternative formulation for the turbulent viscosity compare to the standard k-ε model. The transport equation for the turbulence kinetic energy is same with the standard k-ε model, but the dissipation rate, ε, has been derived from an exact equation for the transport of the mean-square vorticity fluctuation as below.

$$\frac{\partial}{\partial t}(\rho \varepsilon) + \frac{\partial}{\partial x_i}(\rho \varepsilon u_i) =$$

$$\frac{\partial}{\partial x_j} \left[ \left( \mu + \frac{\mu_t}{\sigma_\varepsilon} \right) \frac{\partial \varepsilon}{\partial x_j} \right] + \rho C_1 S \varepsilon - \rho C_2 \frac{\varepsilon^2}{k + \sqrt{\nu \varepsilon}} + C_{1\varepsilon} \frac{\varepsilon}{k} C_{3\varepsilon} G_b + S_\varepsilon \quad (7)$$

#### C. The Standard k-ω Model

The standard k-ω model is also an empirical model based on model transport equations for the turbulence kinetic energy and the turbulent frequency via the relation

$$\mu_t = \rho \frac{k}{\omega} \quad (8)$$

It solves two transport equations, and they are for turbulent kinetic energy, k, and the turbulence frequency, ω. The equations are:

$$\frac{\partial}{\partial t}(\rho k) + \frac{\partial}{\partial x_i}(\rho k u_i) = \frac{\partial}{\partial x_j} \left[ \left( \mu + \frac{\mu_t}{\sigma_k} \right) \frac{\partial k}{\partial x_j} \right] + G_k - \rho \beta^* k \omega \quad (9)$$

$$\frac{\partial}{\partial t}(\rho \omega) + \frac{\partial}{\partial x_i}(\rho \omega u_i) = \frac{\partial}{\partial x_j} \left[ \left( \mu + \frac{\mu_t}{\sigma_\omega} \right) \frac{\partial \omega}{\partial x_j} \right] + \alpha \frac{\omega}{k} G_k - \rho \beta \omega^2 \quad (10)$$

where  $\beta^*$ ,  $\alpha$ ,  $\beta$ , and  $\sigma_\omega$  are model constants.

#### D. The Reynolds Stress Model

The Reynolds stress models are based on transport equations for all components of the Reynolds stress tensor and the dissipation rate. These models do not use the Boussinesq hypothesis, but an equation for the transport equations are solved for the individual stress components. A separate transport equation must be solved for each of the six Reynolds stress components of  $\rho \overline{u_i' u_j'}$ . The differential equation for the transport of the Reynolds stresses is:

$$\frac{\partial}{\partial t}(\rho \overline{u_i' u_j'}) + \frac{\partial}{\partial x_k}(\rho u_k \overline{u_i' u_j'}) = D_{T,ij} + D_{L,ij} + P_{ij} + G_{ij} + \phi_{ij} + \varepsilon_{ij} + F_{ij} \quad (11)$$

where  $D_{T,ij}$  is the turbulent diffusion,  $D_{L,ij}$  is the molecular diffusion,  $P_{ij}$  is the stress production,  $G_{ij}$  is the buoyancy production,  $\phi_{ij}$  is the pressure strain,  $\varepsilon_{ij}$  is the dissipation, and  $F_{ij}$  is the production by system rotation.

#### IV. MODELING AND SIMULATION

The grid generation and CFD calculation were carried out with ANSYS meshing and Fluent codes. As the main objective was to analyze flow characteristics of the orifice plate and to verify whether the velocity profiles at orifice inlet was a fully developed or not, the computational domain was only focused on pipes nearby the orifice plate include two elbows in the same plane.

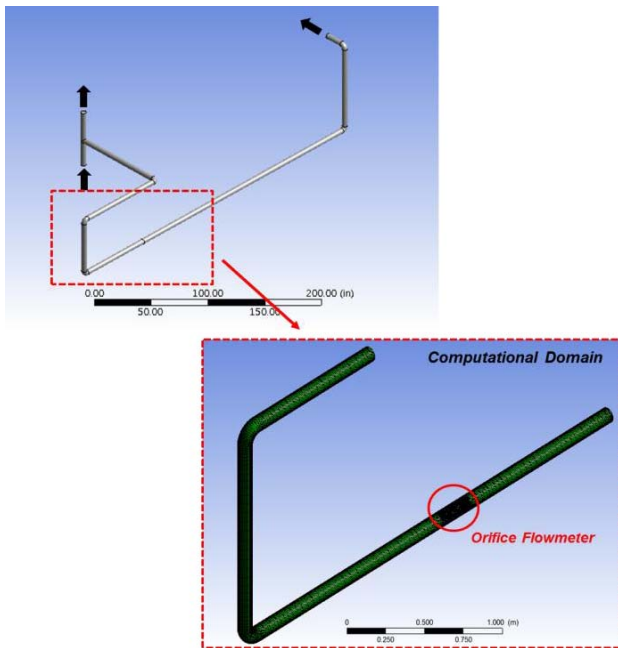


Fig. 2 Computational domain

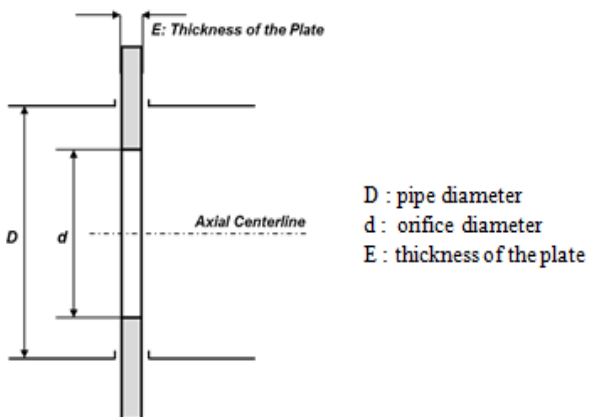


Fig. 3 Geometry information of orifice plate

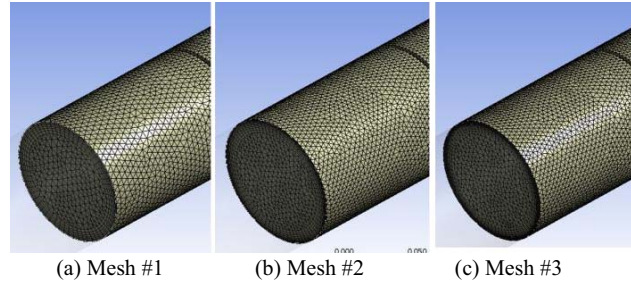


Fig. 4 Grid configuration

TABLE I  
GRID STATISTICS

Statistics	Mesh #1	Mesh #2	Mesh #3
Nodes	166,557	420,648	775,986
Faces	831,058	2,008,117	3,357,769
Cells	342,960	815,844	1,314,686
Average $Y^+$	41.1	13.5	1.0

The computational domain and brief geometry information of the orifice plate is illustrated in Fig. 2 and Fig. 3. The diameters of pipe and orifice are 97.1mm and 72.5mm, the thickness of the plate is 3.18mm, and the straight length on upstream and downstream are about 1.7m and 1.4m, respectively.

##### A. Grid Generation

Three different levels of grid were generated to verify grid-dependency, shown in Fig. 4. Each model consisted of wall boundary layer for considering a suitable near-wall treatment and the corresponding grid size based on the wall  $y^+$ . [5] Mesh statistics for each level is summarized in Table 1. The maximum and average wall  $y^+$  values were calculated under the conditions of 2.27m/s inlet velocity with water.

##### B. Selection of Near-Wall Treatment

Turbulent flows are significantly affected by the presence of walls, where the viscosity-affected regions have large gradients in the solution variables, and accurate presentation of the near wall region determines successful prediction of wall bounded turbulent flow. Therefore, selecting the most suitable near-wall treatment and the corresponding turbulence model are important to obtain accurate results. In this paper, two different types of near-wall treatment (standard wall function or enhanced wall treatment in Fluent) were chosen based on the wall  $y^+$ . That is to say, if the averaged wall  $y^+$  was more than 30, the standard wall function was used, (Mesh #1) and less than 30, the enhanced wall treatment was chosen.

##### C. Evaluation of Grid and Turbulence Model Dependency

For evaluating grid and turbulence model dependency, twelve cases were selected (see Table II); four kinds of turbulence models with proper near-wall treatment for each mesh model. These tests were performed under the same boundary conditions, which were velocity inlet and pressure outlet based on Reynolds number of  $Re \approx 2.2 \times 10^4$ .

TABLE II  
MATRIX OF THE SIMULATIONS

No.	Mesh	Turbulence Model	Near-Wall Treatment
1-1	Mesh #1	Standard $k-\epsilon$	SWF
1-2		Realizable $k-\epsilon$	SWF
1-3		Standard $k-\omega$	None
1-4		Reynolds stress	SWF
2-1	Mesh #2	Standard $k-\epsilon$	EWT
2-2		Realizable $k-\epsilon$	EWT
2-3		Standard $k-\omega$	None
2-4		Reynolds stress	EWT
3-1	Mesh #3	Standard $k-\epsilon$	EWT
3-2		Realizable $k-\epsilon$	EWT
3-3		Standard $k-\omega$	None
3-4		Reynolds stress	EWT

SWF : Standard Wall Function / EWT : Enhanced Wall Treatment

The second order upwind scheme was used for discretization of all governing equations, and the under-relaxation factors were used for all flow parameters for convergence of the solution. The coupling between the pressure and velocity field was established using SIMPLE algorithm. The solutions were converged until the normalized residual is within  $10^{-6}$ .

Table III shows the comparison results of pressure differences through the orifice plate. The quantitative deviations between measurement and calculation were summarized in Table IV. Comparing with the measurement (13.54 kPa), the standard  $k-\epsilon$  model tended to underestimate less than -14.0%, especially the result of an insufficient grid case (Mesh #1; -19.1% underestimated) showed a wide difference. However, the realizable  $k-\epsilon$ , standard  $k-\omega$  and Reynolds stress model using Mesh #2 or #3 give similar matching with experimental data within  $\pm 5\%$  differences. It can be presumed that the standard  $k-\epsilon$  model fails to describe a behavior of turbulent flow nearby wall boundary accurately. The total pressure distribution and streamline make sure this opinion, as illustrated in Fig. 6 and Fig. 7. Each result shows the comparison between the standard  $k-\epsilon$  model and Reynolds stress approach. It can be seen that a recirculation zone in the downstream region of the orifice plate is different. In the case of Reynolds stress model, the detail features of the secondary flow, such as asymmetric recirculation zone and complex eddy motion are well described, while the standard  $k-\epsilon$  model shows a simple symmetric motion.

The deviations in Table IV could be attributed to the limitations of the turbulence model, computational round-off error, uncertainty in the measurement, roughness of pipe, etc.

As for these evaluation results, the Reynolds stress model with Mesh #2 or #3 is recommended for analyzing flow characteristics through the orifice in the auxiliary feedwater system. But, as considering that the Reynolds stress model is needed much higher computational costs which are long computing time and difficulty of convergence than others, the realizable  $k-\epsilon$  model with Mesh #2 or #3 is well-suited for this problem.

TABLE III  
RESULTS FOR PRESSURE DIFFERENCE THROUGH THE ORIFICE PLATE

	Mesh #1 (kPa)	Mesh #2 (kPa)	Mesh #3 (kPa)
Standard $k-\epsilon$	11.0	11.5	11.7
Realizable $k-\epsilon$	12.6	13.4	14.2
Standard $k-\omega$	12.3	13.2	14.2
Reynolds stress	13.0	13.8	13.9

※ Experimental results: 13.54 kPa

TABLE IV  
QUANTITATIVE DEVIATION BETWEEN MEASUREMENT AND CALCULATION

	Mesh #1 (%)	Mesh #2 (%)	Mesh #3 (%)
Standard $k-\epsilon$	-19.1	-15.4	-14.0
Realizable $k-\epsilon$	-6.9	-1.4	4.8
Standard $k-\omega$	-9.3	-2.5	4.5
Reynolds stress	-3.8	1.8	2.4

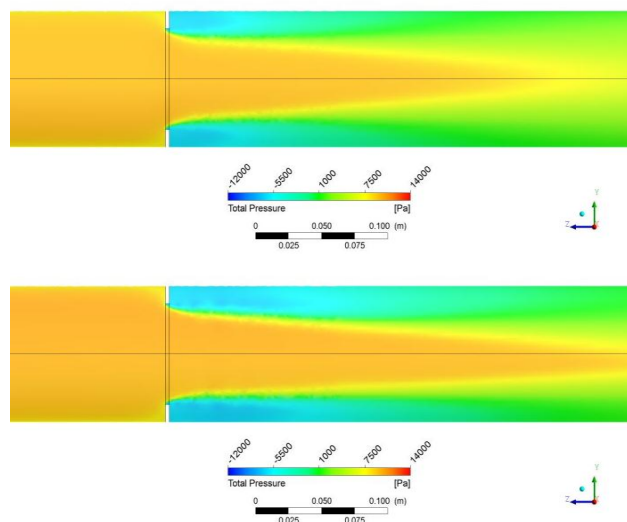
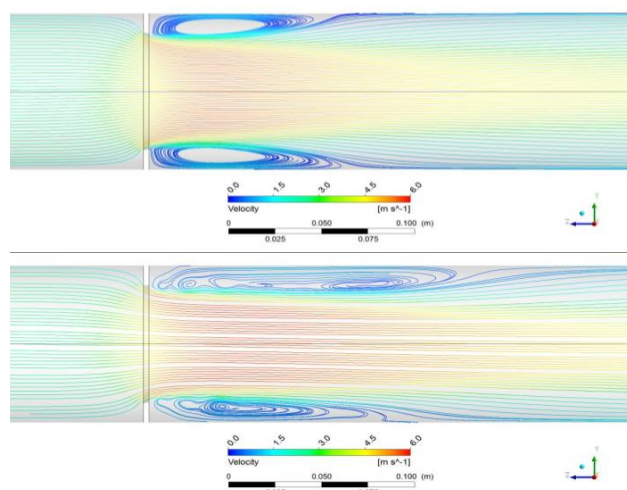
Fig. 6 Total pressure contour of standard  $k-\epsilon$  (top) and RSM (bottom)Fig. 7 Streamline of standard  $k-\epsilon$  (top) and RSM (bottom)

TABLE V  
CALCULATION RESULTS WITH VARIOUS INLET VELOCITIES USING MESH #2

Inlet Velocity (m/s)	Calculations (kPa)	Measurements (kPa)	Deviation (%)
2.26	13.2	13.4	-0.9
3.58	32.9	35.5	-7.1
4.43	49.8	53.7	-7.3
5.54	78.1	83.6	-6.6

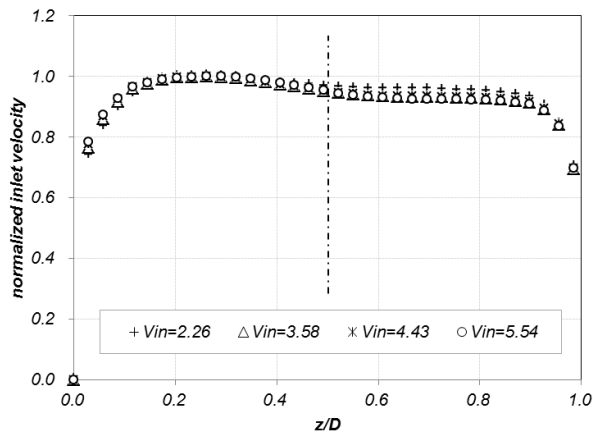


Fig. 8 Velocity profiles at upstream of the orifice using Mesh #2

#### D. Flow Characteristics with Various Inlet Velocities

The predictions of the pressure differences were carried out for various inlet velocities. (2.26, 3.58, 4.43, and 5.54 m/s) As aforementioned, the realizable  $k-\epsilon$  model with enhanced wall treatment was used and grid level was chosen to Mesh #2 and Mesh #3. Except inlet velocity, all other boundary conditions were same with the previous calculation, tests for grid and turbulence model dependency.

The comparison between the predicted results and measurements are presented in Table V and VI. In the case of Mesh #2, only one result in low velocity condition (2.26 m/s) is well predicted and the others have about 7% deviations. The prediction of Mesh #3 shows the opposite tendency, all cases except 2.26 m/s condition are matching within 3% deviations.

The velocity profiles at upstream of the orifice are shown in Fig. 8 and 9. The x-axis indicates a normalized z-direction in cross section of the pipe and y-axis indicates a normalized inlet velocity. Thus, the symmetry based on the middle line means that the inlet flow conditions are sufficiently fully developed; on the contrary, the asymmetry means insufficient conditions.

In this case, it is concluded that the current installation of the orifice is needed more straight upstream pipeline to avoid the flow disturbance which can be causing the distortion in the velocity profile and to measure accurate flow rates.

#### V. CONCLUSION

The present study shows that the realizable  $k-\epsilon$  and the Reynolds stress models with enhanced wall treatment are an appropriate criterion for analyzing flow characteristics through

TABLE VI  
CALCULATION RESULTS WITH VARIOUS INLET VELOCITIES USING MESH #3

Inlet Velocity (m/s)	Calculations (kPa)	Measurements (kPa)	Deviation (%)
2.26	14.1	13.4	+5.1
3.58	35.5	35.5	+0.2
4.43	54.6	53.7	+1.6
5.54	85.7	83.6	+2.5

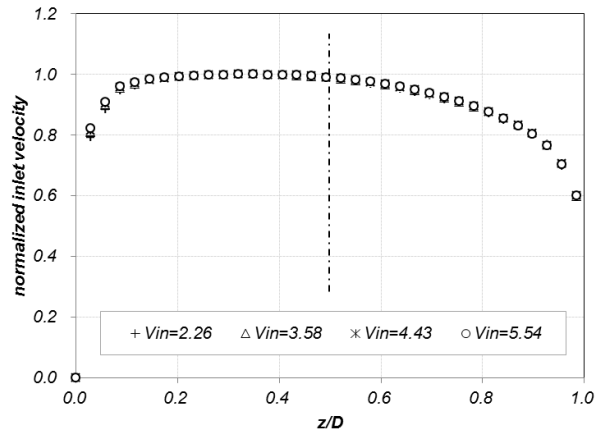


Fig. 9 Velocity profiles at upstream of the orifice using Mesh #3

orifice plate in auxiliary feedwater system of nuclear power plant. It is also advisable that a proper wall  $y^+$  grid size is needed to improve an accuracy and convergence of solution.

#### ACKNOWLEDGMENT

The measurements based on this paper were carried out Korea Hydro and Nuclear Power Company.

#### REFERENCES

- [1] *General Requirements for Fluid Metering: Installation*. USA: ASME PTC 19.5-72, 1972, pp. 179-181.
- [2] *Flow Conditioning and Meter Installation Requirements*. USA: ASME PTC 19.5-2004, 2004, pp. 64-66.
- [3] T. Jinyuan, H.Y. Guan, and L. Chaoqun, *Computation Fluid Dynamics: A Practical Approach*. USA: Butterworth-Heinemann, 2006, pp 35-37.
- [4] Combustion Engineering Technology Cross Training Course Manual. USNRC
- [5] *Fluent Theory Guide*, ANSYS Manual, 2006.